

# Generalization of Wolf Effect of light on Arbitrary Two-Dimensional Surface of Revolution

Chenni Xu, Adeel Abbas, and Li-Gang Wang\*

*Department of Physics, Zhejiang University, Hangzhou 310027, China*

## Abstract

Investigation of physics on two-dimensional curved surface has significant meaning in study of general relativity, inasmuch as its realizability in experimental analogy and verification of faint gravitational effects in laboratory. Several phenomena about dynamics of particles and electromagnetic waves have been explored on curved surfaces. Here we consider Wolf effect, a phenomenon of spectral shift due to the fluctuating nature of light fields, on an arbitrary surface of revolution (SOR). The general expression of the propagation of partially coherent beams propagating on arbitrary SOR is derived and the corresponding evolution of light spectrum is also obtained. We investigate the extra influence of surface topology on spectral shift by defining two quantities, effective propagation distance and effective transverse distance, and compare them with longitudinal and transverse proper lengths. Spectral shift is accelerated when the defined effective quantities are greater than real proper lengths, and vice versa. We also employ some typical SORs, cylindrical surfaces, conical surfaces, SORs generated by power function and periodic peanut-shell shapes, as examples to provide concrete analyses. This work generalizes the research of Wolf effect to arbitrary SORs, and provides a universal method for analyzing properties of propagation compared with that in flat space for any SOR whose topology is known.

PACS numbers: 42.50.Ar, 42.25.Gy, 42.60.Jf, 42.25.Kb

---

\*Electronic address: sxwlg@yahoo.com

## I. INTRODUCTION

A conventional and successful theory to demonstrate gravitational effect is Einstein's general relativity (GR), which creatively relates mass to the geometry of spacetime and provides a significantly different description of gravitation from classical physics. However, some predictions from GR are hard to verify due to the rather faint effects of gravitation. In recent years, there are abundant attempts of physical systems in analogies of astronomical phenomena, which provide ingenious platforms to simulate and explore the theory of GR in laboratory [1–11]. Innovative examples include gravitational black holes in Bose-Einstein condensates [2, 3], gravitational field mimicked in moving dielectric media [5, 6], electromagnetic wormholes [11], etc.

Among these conceptions, one promising idea is to fabricate geometry of a curved spacetime itself with reduced dimensionality. The history of physics on curved surface can be dated back to the early days of quantum mechanics. Historically, two seminal works opened up the researches on curved surface systems from different perspectives: one is to treat problem as entirely two-dimensional (2D) from the beginning and apply canonical quantization approach by DeWitt [12], another is to decouple normal and tangent components of field vector in 3D Schrödinger equation by constraint procedure, therefore reducing problem into 2D by daCosta [13]. It is believed that the curvature of space induces the so-called geometric potential which is determined by both extrinsic and intrinsic curvature. This potential modifies the particles' Hamiltonian and consequently attracts much interest about dynamics of particles on surface in condensed-matter physics [14, 15]. Plenty of applications have been presented especially since new technologies enable the synthesis of nanostructures with complex curved geometry [16–28]. For example, some intriguing phenomena pertinent to electronic states, energy shifts and electron transport have been suggested [21–28].

Dynamics of electromagnetic waves on curved surfaces was carried out in optics about a decade ago [29]. Since then light in curved space has been investigated in various systems [30–40]. For example, wave packets propagating along nongeodesic trajectories on surfaces of revolution (SOR), demonstrating the interaction between curvature and interference effect, is studied both theoretically and experimentally [32, 33]. Topological phases in curved space photonics lattices are also introduced [34]. It is demonstrated that to first order of curvature derivative, a lattice in curved space is equivalent to that in flat space but is subjected to

an extra gauge field. Interestingly, one of curved spaces—the SOR with constant Gaussian curvature, which corresponds to an isotropic and uniform universe, is concretely analyzed [29, 30, 38, 39]. Pioneering experimental works have been done as well by covering a thin layer of waveguide on a 3D object. Properties of beam propagating on such surfaces, such as evolutions of beam width [38] and the second-order degree of coherence [39], are discussed in detail.

In this work, we would like to study the Wolf effect of light on arbitrary 2D curved SORs, which is a generalization of our recent study of light on SOR with constant Gaussian curvature [40]. Wolf Effect refers to the spectral shift of partially coherent polychromatic beams during propagation, which was come up by Wolf in 1980s [41, 42]. This phenomenon arises from the fluctuating (statistical) nature of light sources, and thus is also known as correlation-induced spectral shift [43]. These years have witnessed plenty of studies on Wolf effect in various extended areas [44–48], for example, the scattering system [44], biological tissues [47], inverse scattering problems [48]. Wolf effect has also been experimentally verified in various systems [45–47, 49–53], such as acoustic-correlated system [45, 46] and ordinary partially coherent light sources [49, 50]. However, previous works were focused in flat space. Our recent work demonstrated that the constant Gaussian curvature of space may enhance or suppress the Wolf effect [40].

Nevertheless, the local curvature of space, which is determined by local distribution of mass and energy according to Einstein’s field equation, is not necessarily constant, especially in the areas around massive celestial bodies. Therefore here we are committed to generalize our objects to research the spectral shift of light on arbitrary SORs, and reveals acceleration or deceleration effect of curved space on spectral shift from the perspective of topology of surfaces.

This paper is organized as follows. In Section II, we derive point spread function (PSF) for arbitrary SORs originating from wave equation on curved surface, and give out the expression of output spectrum according to coherence theory. In Section III, a theoretical analysis about the influence of surface topology on longitudinal and transverse spectral shift is given. We develop a technique to compare spectral shifts on such surfaces with that in flat space by defining two quantities, effective propagation distance and effective transverse distance. In Section IV, we employ some typical SORs, cylindrical surfaces, conical surfaces, SORs generated by power function, and a type of periodic peanut-shell shape to illustrate

the theory mentioned above and demonstrate some interesting phenomena. In Section V, we present our concluding remarks.

## II. BASIC THEORY

When being bound on 2D curved surfaces, the propagations of light beams can be described by a 2D scalar wave equation [38]

$$\Delta_g \Phi + (k^2 + H^2 - K)\Phi = 0, \quad (1)$$

where  $\Delta_g = \partial_i(\sqrt{g}g^{ij}\partial_j)/\sqrt{g}$  is the covariant Laplacian,  $g$  is determinant of metric  $g_{ij}$  of curved surfaces, and  $g^{ij} = (\mathbf{g}^{-1})_{ij}$  is element of inverse matrix of  $\mathbf{g}$ ,  $k = k_0 n_0$  is the effective wave number,  $k_0$  is the wave number in vacuum, and  $n_0$  is the refractive index of a thin waveguide-like surface. This equation is derived by decoupling tangential and normal components of 3D vectorial wave equations under neglecting polarization effect. Here  $H$  and  $K$  are extrinsic and intrinsic curvature, respectively, whose effects have been investigated in Ref. [30]. The term  $H^2 - K$ , which is known as geometric potential, shows influence of curved space on wave equation, however, in flat space both  $H$  and  $K$  are vanishing. But for macroscopic cases when the scales of  $H$  and  $K$  are negligible compared with  $k$ , only the intrinsic curvature  $K$  depending on metric will influence the light propagation through the covariant Laplacian  $\Delta_g$ .

Here we consider a sort of special surfaces — generalized SORs, which is formed by rotating a curve on  $Y - Z$  plane with respect to one rotational axis ( $Z$  axis, see Fig. 1). Any SOR can be characterized by its parametrization  $r(t)$ , where  $r$  is known as the radius of revolution (ROR), and  $t$  is the proper length along the curve. There are two methods to parametrize such surfaces. The first one is to directly come up with the relation between  $r$  and  $t$ . Another method is to first obtain the expression of generatrix in  $Y - Z$  plane,  $Z = f(Y)$ , and then calculate  $r(t)$  according to mathematical relation, where  $f$  is a monotonic function. One can obtain the underlying line element  $ds^2 = g_{ij}dx^i dx^j = dt^2 + r^2(t)d\theta^2 = dt^2 + r^2(t)/r_0^2 d\varepsilon^2$  for such surfaces. Here  $r_0$  is the ROR at  $t = 0$ , and  $\varepsilon \equiv r_0\theta$  is the transverse proper length of the initial circle of latitude defined for further discussion. Attention should be paid that  $r(t)$  is already the most general form of metric since it can be an arbitrary form corresponding to different SORs.

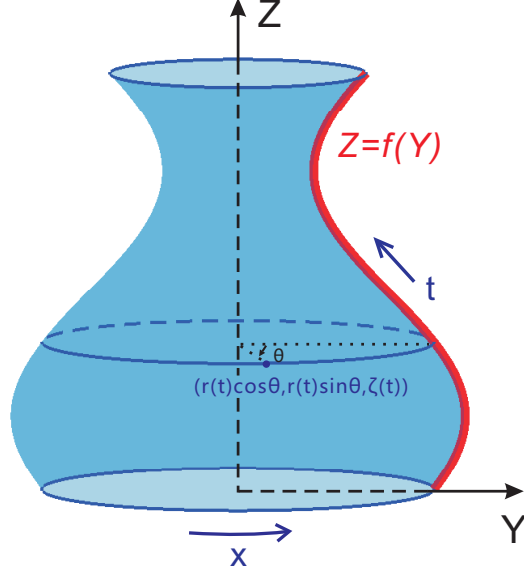


FIG. 1: (Color online) Sketch of surface of revolution. SOR is generated by rotating generatrix (denoted by red solid line) in  $Y - Z$  plane with respect to  $Z$  axis, and  $r(t)$  is radius of rotation and  $\theta$  is rotation angle. Different expression of  $r(t)$  will lead to different topology of SOR.

With the metric  $g_{ij}$ , one can obtain the 2D wave equation on an SOR as follows

$$\frac{\partial^2 \Phi(\varepsilon, t)}{\partial t^2} + \frac{r'(t)}{r(t)} \frac{\partial \Phi(\varepsilon, t)}{\partial t} + \frac{r_0^2}{r^2(t)} \frac{\partial^2 \Phi(\varepsilon, t)}{\partial \varepsilon^2} + k^2 \Phi(\varepsilon, t) = 0, \quad (2)$$

where  $r'(t)$  is the first derivative of  $r(t)$  with respect to  $t$ ,  $H^2$  and  $K$  are omitted when  $k^2 \gg H^2, K$ . For beams starting from  $t = 0$  along the longitudinal direction, substitute the ansatz  $\Phi = Ar^{-1/2}(t)u(t, \varepsilon) \exp(ikt)$  into Eq. (2), where  $A$  is a constant and  $u(t, \varepsilon)$  is the complex amplitude of slowly varying envelope. Thus, by applying the paraxial approximation  $\partial^2 u(t, \varepsilon) / \partial t^2 \ll 2ik \partial u(t, \varepsilon) / \partial t$ , Eq. (2) evolves into

$$2ik \frac{\partial u(t, \varepsilon)}{\partial t} + V_{\text{eff}}(t)u(t, \varepsilon) + \frac{r_0^2}{r^2(t)} \frac{\partial^2 u(t, \varepsilon)}{\partial \varepsilon^2} = 0, \quad (3)$$

where

$$V_{\text{eff}}(t) = \frac{1}{4r^2(t)} \left[ \frac{dr(t)}{dt} \right]^2 - \frac{1}{2r(t)} \frac{d^2 r(t)}{dt^2} \quad (4)$$

is the effective potential intrinsically induced by the curvature of surface. By separating the phase  $u(t, \varepsilon) = v(t, \varepsilon) \exp \left[ \frac{i}{2k} \int_0^t V_{\text{eff}}(t') dt' \right]$  and defining a new physical quantity

$$\Xi(t) = \int_0^t \frac{r_0^2}{r^2(t')} dt'. \quad (5)$$

Eq. (3) can be further simplified to

$$2ik\frac{\partial v(t, \varepsilon)}{\partial \Xi} + \frac{\partial^2 v(t, \varepsilon)}{\partial \varepsilon^2} = 0, \quad (6)$$

which is the standard 1D Schrödinger equation. By solving Eq. (6), the normalized point spread function (PSF) can be obtained

$$h(\varepsilon, \varepsilon', t) = \sqrt{\frac{kr_0}{i2\pi\Xi r(t)}} \exp\left[\frac{ik(\varepsilon - \varepsilon')^2}{2\Xi}\right] \\ \times \exp\left[ikt + \frac{i}{2k} \int_0^t V_{\text{eff}}(t') dt'\right]. \quad (7)$$

Here  $\varepsilon$  is the abscissa at source plane ( $t = 0$ ) and  $\varepsilon'$  is the abscissa at any plane ( $t > 0$  or  $t < 0$ ) during propagation, and  $\{kr_0/[i2\pi\Xi r(t)]\}^{1/2}$  is the normalized coefficient. Before moving to next step, let us first look at the PSF in flat space, which is usually expressed as

$$h_f(\varepsilon_f, \varepsilon'_f, z_f) = \sqrt{\frac{k}{i2\pi z_f}} \exp(ikz_f) \\ \times \exp\left[\frac{ik}{2z_f}(\varepsilon_f^2 - 2\varepsilon_f\varepsilon'_f + \varepsilon'^2_f)\right], \quad (8)$$

where the subscript f, denoting the flat space, is used to avoid ambiguousness, and  $z_f$  is the propagating distance in flat (or free) space. Comparing Eq. (7) with Eq. (8), one can find there is an extra phase induced by surface in Eq. (7). Besides,  $z_f$  in Eq. (8) is substituted by quantity  $\Xi$  in Eq. (7). Therefore, the newly-defined quantity  $\Xi$  can be regarded as the effective propagation distance, although it intrinsically corresponds to the coordinate transformation of propagation distance  $t$ .

According to coherence theory, by using PSF of Eq. (7), the output cross-spectral density at arbitrary plane  $t \neq 0$  can be expressed as

$$W_{\text{out}}(\varepsilon'_1, \varepsilon'_2, t, \omega) = \langle \Phi_{\text{out}}(\varepsilon'_1, t, \omega) \Phi_{\text{out}}^*(\varepsilon'_2, t, \omega) \rangle \\ = \iint d\varepsilon_1 d\varepsilon_2 W_{\text{in}}(\varepsilon_1, \varepsilon_2, 0, \omega) \\ \times h(\varepsilon_1, \varepsilon'_1, t) h^*(\varepsilon_2, \varepsilon'_2, t). \quad (9)$$

Here we assume that the initial light source is a well-collimated narrow beam, with a beam half-width  $\sigma_s$ , being incident on a macroscopic surface. When  $\sigma_s \ll |2\pi r_0|$ , the intergral interval can be mathematically expanded to  $(-\infty, +\infty)$ . Without loss of generality, the

incident partially coherent source here is described by a polychromatic Gaussian Schell-model beam

$$W_{\text{in}}(\varepsilon_1, \varepsilon_2, 0, \omega) = S_i(\omega) \exp\left(-\frac{\varepsilon_1^2 + \varepsilon_2^2}{4\sigma_s^2}\right) \times \exp\left[-\frac{(\varepsilon_1 - \varepsilon_2)^2}{2\sigma_g^2}\right], \quad (10)$$

where  $S_i(\omega)$  is initial spectrum,  $\sigma_s$  is the initial beam half-width and  $\sigma_g$  is the initial correlation length of the source. Correspondingly the output spectrum at any observation point can be obtained after tedious calculation

$$S_{\text{out}}(x, t, \omega) \equiv W_{\text{out}}(\varepsilon', \varepsilon', t, \omega) = \frac{S_i(\omega)}{\Omega(t, \omega)} \exp\left[-\frac{x^2}{2\sigma_s^2\Omega^2(t, \omega)}\right], \quad (11)$$

where

$$\Omega(t, \omega) = \alpha[1 + \Xi^2/Z_R^2(\omega)]^{1/2} \quad (12)$$

is the beam-expansion coefficient on arbitrary SOR,  $\alpha = r(t)/r_0$  is the ratio of the ROR at  $t > 0$  to the ROR at  $t = 0$  and is known as expansion ratio,  $x = \alpha\varepsilon'$  is the proper transverse length of surface at  $t > 0$ , and  $Z_R(\omega) = 2k\sigma_s^2/[1 + 4\sigma_s^2/\sigma_g^2]^{1/2} = 2(\omega n_0/c)\sigma_s^2/[1 + 4\sigma_s^2/\sigma_g^2]^{1/2}$  is the frequency-dependent Rayleigh distance of light beam. Note that in Eq. (9), the second exponential in Eq. (7) will be counteracted with its conjugate. Therefore the curvature-induced effective potential  $V_{\text{eff}}$  does not exert influence on the output spectrum as well as spectral shift.

### III. GENERAL BEHAVIORS OF SPECTRAL SHIFT

In the following discussion, the initial spectrum  $S_i(\omega)$  of light is assumed to be a single peak, e.g, a Gaussian or Lorentz-type spectral line, with its spectral line-width  $\delta$  being much smaller than its center frequency  $\omega_0$  (i.e.,  $\delta \ll \omega_0$ ). In this sense, one can safely suppose the output spectrum still has only a single peak with a negligible distortion, then its new center frequency  $\omega'_0$  via spectral shift must satisfy  $\partial S_{\text{out}}(x, t, \omega)/\partial\omega|_{\omega=\omega'_0} = 0$ . From Eq. (11), one can obtain

$$\frac{S'_i(\omega'_0)}{S_i(\omega'_0)} + \frac{\Omega'(t, \omega'_0)}{\Omega(t, \omega'_0)} \left[ \frac{x^2}{\sigma_s^2\Omega^2(t, \omega'_0)} - 1 \right] = 0, \quad (13)$$

where  $S'_i(\omega'_0)$  and  $\Omega'(t, \omega'_0)$  denote the first derivatives versus  $\omega$  at  $\omega'_0$ . This equation has the same form as Eq. (10) in our previous investigation [40], but the main differences are the function  $\Omega(t, \omega)$  and its derivative  $\Omega'$ , which are now generalized to any SOR. Spectral shift  $\Delta\omega$  is calculated by  $\Delta\omega = \omega'_0 - \omega_0$ . By solving Eq. (13), in principle, one can obtain spectral shift at every spatial point on any curved SOR, although it is too complex to give out an analytical solution. Here we present another method by comparing the effect of curved surface on spectral shift with the situations in flat space. Rewrite Eq. (13) as

$$\frac{x^2}{\alpha^2 \sigma_s^2 \Lambda^2(\Xi, \omega'_0)} = 1 - \frac{S'_i(\omega'_0) \Lambda(\Xi, \omega'_0)}{S_i(\omega'_0) \Lambda'(\Xi, \omega'_0)}, \quad (14)$$

where  $\Lambda(\Xi, \omega'_0) = [1 + \Xi^2/Z_R^2(\omega'_0)]^{1/2} > 0$ , and  $\Lambda'(\Xi, \omega'_0) = -\Xi^2/[\omega'_0 Z_R^2(\omega'_0) \Lambda(\Xi, \omega'_0)] < 0$ . The correspondence in flat space is (the detailed calculation is similar to previous one and is omitted)

$$\frac{x_f^2}{\sigma_s^2 \Lambda_f^2(z_f, \omega'_0)} = 1 - \frac{S'_i(\omega'_0) \Lambda_f(z_f, \omega'_0)}{S_i(\omega'_0) \Lambda'_f(z_f, \omega'_0)}, \quad (15)$$

where  $\Lambda_f(z_f, \omega'_0) = [1 + z_f^2/Z_R^2(\omega'_0)]^{1/2}$ . From Eq. (14) and Eq. (15), we can find that the transverse distance  $x_f$  on the left-hand side of Eq. (15) is substituted by  $x/\alpha$  on curved surface. Actually we have known that

$$\varepsilon' = x/\alpha. \quad (16)$$

Thus, in this sense,  $\varepsilon'$  in Eq. (11) might be seen as the effective transverse distance, but it is not a real length on curved surfaces. Besides, on right-hand side of Eq. (15), the longitudinal propagation distance  $z_f$  in flat space is substituted by the effective propagation distance  $\Xi$  of Eq. (14) in curved space (defined in Section II). In the form of  $\Xi$  and  $\varepsilon'$ , Eq. (14) is mathematically equivalent to Eq. (15). Therefore, we can find that when the value of  $\Xi > t$ , compared with flat space, longitudinal spectral shift is accelerated, and vice versa. When the value of  $\varepsilon' > x$ , transverse spectral shift is accelerated, and deceleration effect happens when  $\varepsilon' < x$ .

As is discussed in Ref. [40], longitudinally central frequency of output spectrum moves towards higher frequency (i.e., the spectral shift is under tendency of blue shift), while along transverse direction, central frequency tends to move towards lower frequency (i.e., tendency of red shift). Thus, for on-axis points where both  $x$  and  $\varepsilon'$  equal to zero, spectral shift is free from transverse squeeze of topology of surfaces. Since  $S'_i(\omega'_0) \Lambda(\Xi, \omega'_0) = S_i(\omega'_0) \Lambda'(\Xi, \omega'_0) < 0$ ,

only blue shift occurs and increases with propagation distance. However, there is an upper limit which can be calculated by setting  $t \rightarrow \infty$  in Eq. (13). In general, after a long propagation, effective propagation distance  $\Xi$  is large enough so that

$$\Xi^2/Z_R^2(\omega'_0) \gg 1. \quad (17)$$

Therefore, Eq. (13) can be further simplified into

$$\frac{1}{\omega'_0} + \frac{S'_i(\omega'_0)}{S_i(\omega'_0)} = 0. \quad (18)$$

The solution of Eq. (18), which corresponds to the maximal blue shift, is independent of topology of surface and the initial parameters of beam, but it only depends on the incident profile of spectrum. Nevertheless, for few SORs, the relation (17) may not be valid, such as the conical surface which will be mentioned in Section IV, thus Eq. (18) cannot be used for these surfaces. For those exceptions, the maximal blue shift can only be calculated by Eq. (13), and therefore it is determined by topology of surface, initial parameters of beams and incident profile of spectrum.

For off-axis points where  $x$  and  $\varepsilon'$  do not equal to zero, when  $\varepsilon'^2 = \sigma_s^2 \Lambda^2(\Xi, \omega'_0)$  or  $x^2 = \alpha^2 \sigma_s^2 \Lambda^2(\Xi, \omega'_0)$ , then one can obtain  $S'_i(\omega'_0) = 0$ , i.e.,  $\omega'_0 = \omega_0$  for a single-peak spectral line. This indicates that for the observation points along the curves of  $\varepsilon'^2 = \sigma_s^2 \Lambda^2(\Xi, \omega_0)$  [or  $x^2 = \alpha^2 \sigma_s^2 \Lambda^2(\Xi, \omega_0)$ ], there is no spectral shift. When  $\varepsilon'^2 < \sigma_s^2 \Lambda^2(\Xi, \omega'_0)$  or  $x^2 < \alpha^2 \sigma_s^2 \Lambda^2(\Xi, \omega'_0)$ , one can also find  $S'_i(\omega'_0) < 0$  from Eq. (14). Thus  $\omega'_0 > \omega_0$  and it indicates blue shift happens. When  $\varepsilon'^2 > \sigma_s^2 \Lambda^2(\Xi, \omega'_0)$  or  $x^2 > \alpha^2 \sigma_s^2 \Lambda^2(\Xi, \omega'_0)$ , one can find  $S'_i(\omega'_0) > 0$ . This tells  $\omega'_0 < \omega_0$  and red shift happens.

#### IV. EXAMPLES OF SOME TYPICAL SORS

In order to provide a concrete demonstration as well as a reasonable verification of theories mentioned above, several examples about spectral shift on some SORS will be given in this section. Specifically speaking, both monotonous surfaces (i.e., the corresponding generatrices are monotonic and hence the surfaces either contract or expand) and periodic surfaces (i.e., the corresponding generatrices are non-monotonic and the surfaces contract and expand periodically) are investigated. In the former case, we analyze and proof the effect of surface by comparing longitudinal and transverse spectral shifts on such surfaces with different

power exponents. While in the latter case some interesting phenomena occur on account of periodicity. Without loss of generality, in the following contents initial spectral profile will be Gaussian, i.e.,  $S_i(\omega) = \exp[-(\omega - \omega_0)^2/(2\delta^2)]/(\delta\sqrt{2\pi})$ , where  $\delta$  is its line-width.

### A. Cylindrical Surface

The ROR of a cylindrical surface is identical everywhere, i.e.,  $r(t) = r_0$  for arbitrary distance  $t$ , therefore the effective propagation distance is

$$\Xi = \int_0^t \frac{r_0^2}{r^2(t')} dt' = t, \quad (19)$$

which is exactly same as the case in flat space. Meanwhile one has always the expansion ratio  $\alpha = 1$ . Accordingly, beam width, behavior of longitudinal and transverse spectral shift are all the same as that in flat space as well. Actually the line element of a cylindrical surface is  $ds^2 = dt^2 + d\varepsilon^2$ , which is also used to describe the flat surface.

### B. Conical Surface

Since the apex of cone is a singularity which cannot be chosen as the initial circle of abscissa, we should first choose an initial position where the corresponding ROR  $r = r_0$  to establish the curvilinear coordinate system and propagate the beam (As is proved in Appendix, for beams propagating with same trajectory on the same conical surface, however we establish the coordinate will not influence the result). In chosen coordinate, there may be two cases for the relations between ROR  $r(t)$  and longitudinal coordinate  $t$  for conical surfaces as follows

$$\text{Case 1: } r(t) = r_0 + \frac{1}{\sqrt{1+m^2}}t \text{ for } t \in [0, \infty) \quad (20)$$

$$\text{Case 2: } r(t) = r_0 - \frac{1}{\sqrt{1+m^2}}t \text{ for } t \in [0, r_0\sqrt{1+m^2}) \quad (21)$$

where  $m > 0$  is the absolute value of the slope of the generatrix. Now the effective propagation distance can be calculated by

$$\Xi = \int_0^t \frac{r_0^2}{r^2(t')} dt' = \frac{r_0 t}{r_0 \pm \frac{1}{\sqrt{1+m^2}}t}. \quad (22)$$

In the case 1, it is clearly seen that when  $t \rightarrow \infty$ ,  $\Xi$  tends to a finite value  $r_0\sqrt{1+m^2}$  although the conical SOR is expanded to infinity. It means that its effective distance approaches a fixed value only determined by its initial ROR and slope of the generatrix. Since  $\Xi < t$  and  $\varepsilon' < x$ , both the longitudinal and transverse spectral shifts are decelerated. Furthermore, Eq. (18) mentioned in Section III is not valid, and the maximal blue shift should be calculated by Eq. (13). In the case 2, as  $t \rightarrow r_0\sqrt{1+m^2}$ ,  $\Xi$  tends to be infinity. Because of  $\Xi > t$  and  $\varepsilon' > x$ , both the longitudinal and transverse spectral shifts are accelerated.

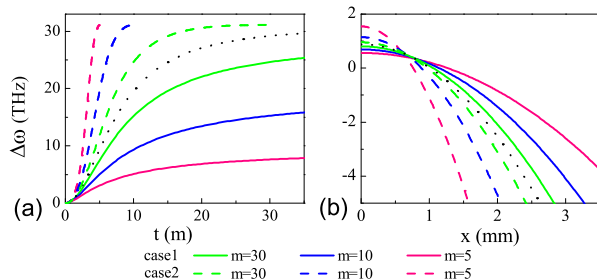


FIG. 2: (Color online) Behaviors of longitudinal (a) and transverse (b) spectral shifts on conical surfaces with different slopes at (a)  $x=0$  and (b)  $t=1.3$  m. On each surface, propagation starts from positions where ROR  $r_0 = 1$  m. Other parameters are  $\omega_0 = 2\pi \times 500$  THz,  $\delta = 0.1\omega_0$ ,  $\sigma_s = 1$  mm,  $\sigma_g = 0.5$  mm, and  $n_0 = 1.51$ . Note that black dot lines denote the case in flat space.

Figure 2 plots both longitudinal and transverse spectral shifts on conical surfaces with different slope  $m$ . It is easily observed from Fig. 2 (a) that for on-axis points, spectral shifts on surfaces of case 2 increase faster than that in flat space, and tend to a same maximal blue shift. While on surfaces of case 1 spectral shifts increase slower than flat space, and the corresponding maximal blue shifts, which are always smaller than that in the case 2, vary with slopes of conical surfaces. From Fig. 2 (b) it is also proved that transverse spectral shifts on surfaces in the case 1 evolve slower, and are accelerated on surfaces in the case 2. Besides, spectral shift evolves faster with the increase of  $m$  in both longitudinal and transverse direction in the case 1, and with the decrease of  $m$  in the case 2.

### C. SORs generated by power function

Now let us consider some more complex SORs. In the  $Y - Z$  plane of Fig. 1, the expression of generatrix can be given by power function,  $Z = Y^p - r_0^p$  with  $Y > 0$ , where

$r_0 > 0$  is the initial ROR at  $t = 0$  and  $p \neq 0$  is a non-zero real number. On  $Y - Z$  plane, the relation  $(dY/dt)^2 + (dZ/dt)^2 = 1$  is geometrically valid, and distance from points on generatrix to axis of revolution ( $Z$  axis), i.e., the ROR  $r(t)$  constantly equals to  $|Y|$ . By substituting expression of power function, relation between  $r$  and  $t$  is acquired

$$t = \int_{r_0}^r \sqrt{1 + p^2 Y^{2p-2}} dY \equiv G(r), \quad (23)$$

where  $G$  is the function after integral on the right-hand side. The form of parametrization  $r(t)$  can be obtained by solving the inverse function of Eq. (23), i.e.,  $r(t) = G^{-1}(t)$ .

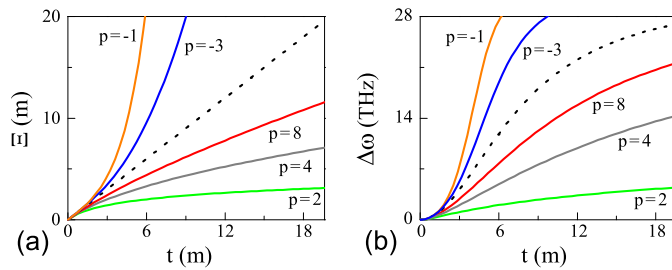


FIG. 3: (Color online) (a) Effective propagation distance and (b) longitudinal spectral shift versus propagation distance  $t$  for five typical SORs generated by power function ( $p = -3, -1, 2, 4$  and  $8$ ). For better comparison, situation of flat space is also plotted by black dot line. Other parameters are  $r_0 = 1$  m,  $\omega_0 = 2\pi \times 500$  THz,  $\delta = 0.1\omega_0$ ,  $\sigma_s = 1$  mm,  $\sigma_g = 0.5$  mm,  $n_0 = 1.51$ .

Spectral shift versus propagation distance  $t$  of on-axis points on such surfaces with different power exponent  $p$  is illustrated in Fig. 3(b). To make the analysis more convincing, initial ROR is chosen to be equal to 1 m. It can be observed that on-axis longitudinal spectral shift on surfaces with negative  $p$  increases faster than that in flat space (denoted by black dot line in figure), and it increases slower on surfaces with positive  $p$  when compared with flat space. Besides, longitudinal spectral shift increases faster with the increase of  $p$  both when  $p > 0$  and  $p < 0$ . This phenomenon can be explained as follows. For on-axis points, since  $\varepsilon' = x = 0$ , only longitudinal effect of surface, to be specific, the relation between effective propagation distance  $\Xi$  and real propagation distance  $t$ , should be taken into consideration. As is shown in Fig. 3(a), effective propagation distance  $\Xi$  in flat space is smaller than that on such SORs with negative  $p$ , and greater than that on such SORs with positive  $p$ . Both when  $p > 0$  and  $p < 0$  effective propagation distance  $\Xi$  is larger with the increase of  $p$ , leading to faster spectral shift in Fig. 3(b). The information in Fig. 3(a) can

also be obtained analytically. For SOR with  $p > 0$ , surface is expanding, i.e., ROR increases over  $t$ . Therefore expansion ratio  $\alpha$  is greater than 1, and the corresponding effective propagation distance  $\Xi$  is less than its real counterpart, so longitudinal spectral shift is depressed compared with flat space. For SOR with  $p < 0$ , on the contrary, surface is contracting, and effective propagation distance  $\Xi$  is greater than its real counterpart, and longitudinal spectral shift is accelerated. Besides, with greater  $p$ , ROR  $r(t)$  increases slower with  $t$  when  $p > 0$  and decreases faster with  $t$  when  $p < 0$ , which leads to smaller expansion ratio  $\alpha$ , and greater effective propagation distance.

For off-axis points, as the effective transverse distance is no longer vanishing, its spectral shift will be subjected to both transverse and longitudinal stretch and contraction from surface. In Fig. 4 three representatives of such SORs ( $p = -1$ : Gabriel's horn,  $p = 1$ : conical surface,  $p = 2$ : paraboloid) along with cylindrical surface are listed to display the longitudinal spectral shifts at different transverse positions ( $x = 0, 1 \text{ mm}, 1.5 \text{ mm}, 2 \text{ mm}, 2.5 \text{ mm}$ ). In Figs. 4(a2, b2, c2, d2), it is found that in transverse direction where  $x$  coordinate increases, spectral shift tends to develop towards red shift. Along propagation, absolute value of red shift first increases and then decreases, in some cases it decreases till zero and transfers to blue shift. It is because that from its definition, effective propagation distance  $\Xi$  is a quantity that reveals the accumulative effect of trajectory which beam passes. At areas where longitudinal coordinate  $t$  are relatively small, difference between effective propagation distance and real propagation distance (proper length) are not distinct, and thus longitudinal effect of surface is not obvious and transverse effect plays dominating role. With the increase of propagation distance, longitudinal effect of surface intensifies and spectral shift starts to develop towards blue shift, which gives rise to a “dip” structure.

Comparing Figs. 4(a2, b2, c2, d2), one may notice that spectral (red) shift along transverse direction in Fig. 4(a1) near the “dip” structure evolves fastest among all the four SORs, then follow the cylindrical surface, paraboloid and conical surface (for example, at  $x = 2.5 \text{ mm}$ , the greatest absolute value of red shift on Gabriel' horn is approximately 1400 THz, and approximately 30 THz on cylindrical surface, approximately 0.9 THz on paraboloid, approximately 0.2 THz on conical surface). It is because for Gabriel' horn and actually all such SORs with  $p < 0$ , surface is contracting and expansion ratio  $\alpha$  is less than 1, transverse (red) spectral shift is drastically accelerated. While for SORs with  $p > 0$ , surface is expanding and expansion ratio is greater than 1, transverse (red) spectral shift

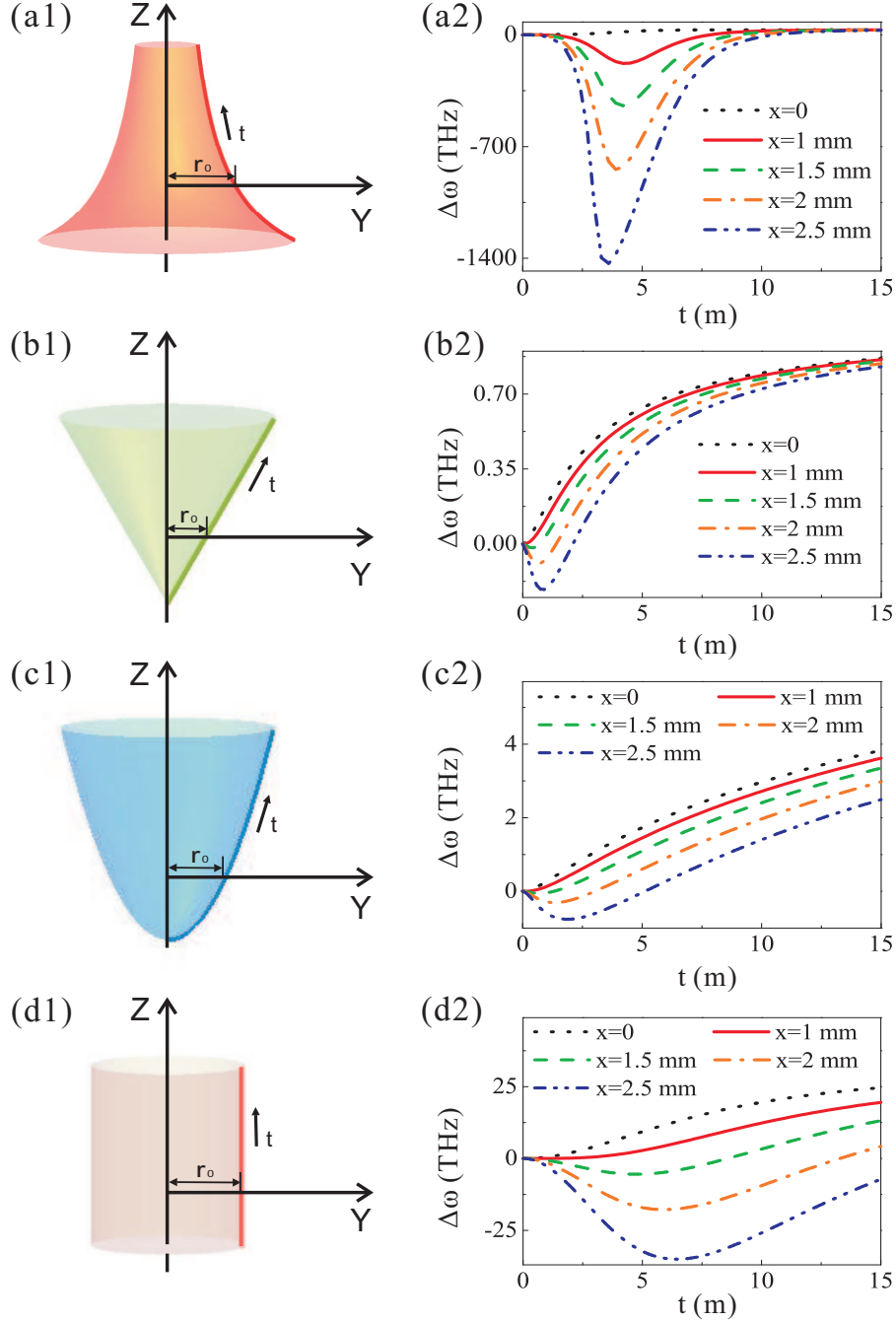


FIG. 4: (Color online) Comparison about distributions of spectral shifts between three typical SORs generated by generalized power function. (a1)-(d1) Shape of such SORs with  $p = -1$  (a1), 1 (b1), 2 (c1) together with corresponding generatrices. For better comparison, situation on cylindrical surface, which is proved to be equivalent to flat space, is also plotted (d1). (a2-d2) The corresponding longitudinal spectral shifts with respect to propagation distance  $t$  at different transverse coordinates  $x = 0, 1$  mm, 1.5 mm, 2 mm, 2.5 mm on the corresponding surfaces. Both the on-axis longitudinal spectral shift and situation of transverse spectral shift can be analyzed from these figures. In (a2) - (d2), other parameters are the same as Fig. 3.

evolves slower than that on flat space. And with the increase of  $p$ , ROR increases slower with  $t$ , leading to a faster transverse spectral shift.

#### D. Periodic peanut-shell shape (PPSS)

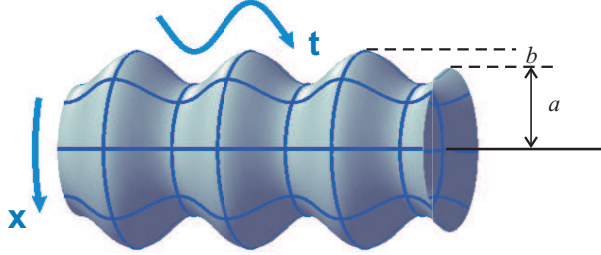


FIG. 5: (Color online) Schematic illustration of periodic peanut-shell shape. Curvilinear coordinates  $t$  and  $x$  are marked on surface by blue lines. Parameters  $a$  and  $b$  denote average radius of surface and roughness on surface, respectively.

In this subsection, we are going to introduce a type of periodic structures on which intriguing phenomena occur, as shown in Fig. 5. For the sake of convenience, we adopt the name “periodic peanut-shell shape” from Ref. [23] to refer this structure, which here is parametrized as

$$r(t) = a - b \cos(t/R + \varphi_0) \quad (24)$$

with  $a > b$ . Here structure parameter  $a$  determines the average radius of the surface, while  $b$  describes undulated amplitude of the surface,  $0 \leq \varphi_0 \leq \pi$  determines the initial situation of surface at  $t = 0$ , and  $R$  denotes the longitudinal extension of the sags and crests on surface. Its effective propagation distance is complex but can be given by

$$\Xi(t) = \gamma_1 [m\pi + \tan^{-1} \beta_t - \tan^{-1} \beta_0] - \frac{Q \sin(t/2R)}{r(t)}, \quad (25)$$

where  $\gamma_1 = 2aR(a - b \cos \varphi_0)^2 / (a^2 - b^2)^{3/2}$ ,  $\beta_t = (\frac{a+b}{a-b})^{1/2} \tan[(t/R + \varphi_0)/2]$ ,  $\beta_0 = (\frac{a+b}{a-b})^{1/2} \tan[\varphi_0/2]$ ,  $Q = 2bR(a - b \cos \varphi_0)[b \cos(t/2R) - a \cos(t/2R + \varphi_0)] / (a^2 - b^2)$ , and  $m = \lfloor \lfloor \frac{1}{\pi}(t/R + \varphi_0) \rfloor + 1 \rfloor / 2$  with the symbol “[ $\cdot$ ]” being a floor function. As shown in the previous subsections, this quantity  $\Xi(t)$  determines the relative spectral shift along the on-axis propagation.

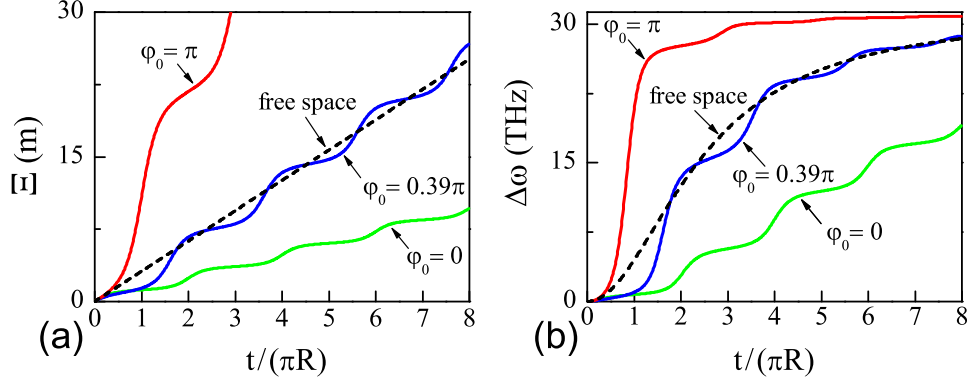


FIG. 6: (Color online) (a) Effective propagation distance and (b) on-axis longitudinal spectral shift of PPSSs with three different initial phases  $\varphi_0 = 0, 0.39\pi$  and  $\pi$ . For better comparison, situation in flat space is plotted in black dashed line. Other parameters are  $a = 2$  m,  $b = 1$  m,  $R = 1$  m,  $\omega_0 = 2\pi \times 500$  THz,  $\delta = 0.1\omega_0$ ,  $\sigma_s = 1$  mm,  $\sigma_g = 0.5$  mm,  $n_0 = 1.51$ .

Figure 6 demonstrates three typical cases of such surfaces for different  $\varphi_0$ . The corresponding behaviors of the spectral shift  $\Delta\omega$  along the on-axis propagation are plotted in Fig. 6(b). For example, when  $\varphi_0 = 0$ , one always has  $\Xi < t$ , which indicates that the total spectral shift  $\Delta\omega$  along the propagating axis is smaller than that in flat space. When  $\varphi_0 = 0.39\pi$ , both the lines of  $\Xi$  and  $t$  may intercross together, which leads to the effect that the total spectral shift  $\Delta\omega$  along the on-axis propagation in certain distances is larger than that in flat space and it may also be smaller than that in flat space in other distances. When  $\varphi_0 = \pi$ , since  $\Xi > t$  is always hold, spectral shift  $\Delta\omega$  on the on-axis propagation in such cases is always larger than that in flat space.

Figure 7 demonstrates distributions of spectral shifts  $\Delta\omega$  on such surfaces with three different initial phases  $\varphi_0$ , with effect of undulation on surface being considered. The boundary between blue-shift and red-shift area (denoted by black dashed line in each subfigure), where zero spectral shift occurs and is known as no-shift line [40], reveals a shape of periodic expansion and contraction during propagation, although the overall tendency is to expand, that is, the blue-shift area tends to enlarge during propagation. By comparing Figs. 7(a1-a3) (or Figs. 7(b1-b3), or Figs. 7(c1-c3), without loss of generality, in the following contents we will take Figs. 7(a1-a3) as example), it is observed that with the increase of undulation parameter  $b$  (that is, the undulating structure on surface is more prominent in contrast to its average radius), amplitude of oscillation of no-shift line becomes more drastic. By com-

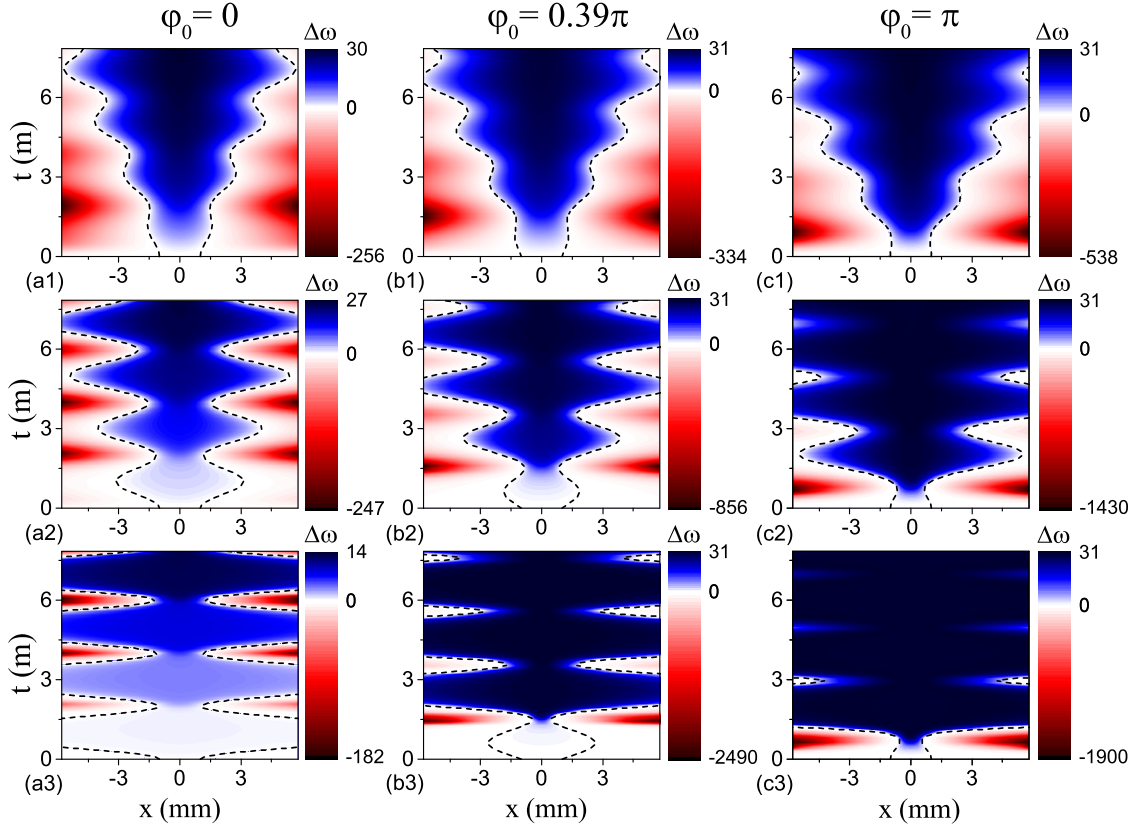


FIG. 7: (Color online) Distribution of spectral shift  $\Delta\omega$  (THz) with different undulation on PPSSs with three different initial phases (a1-a3)  $\varphi_0 = 0$ , (b1-b3)  $\varphi_0 = 0.39\pi$ , (c1-c3)  $\varphi_0 = \pi$ , Here  $a = 2$  m,  $R = 1.9$  m, and undulation parameter  $b$  are (a1-c1)  $b = 0.3$  m, (a2-c2)  $b = 1$  m, (a3-c3)  $b = 1.7$  m. Other parameters are same as those in Fig. 6.

paring Figs. 7(a1-a3), one can also observe that near areas where contraction of no-shift line is greatest, that is,  $t = 2\pi R, 4\pi R, 6\pi R, \dots$ , on-axis blue shift increases faster than other areas. It is very obvious in Fig. 7(a3), where blue shift increases rapidly whenever beam passes such positions and remains ignorable in each period. Besides, in transverse direction, it takes shorter distance to transfer from blue-shift area to red-shift area, and the absolute value of red shift is greater in these areas. In conclusion, spectral shift will experience a runup at positions where no-shift line contracts most, and this phenomenon is more significant when undulation parameter  $b$  increases. It is because that these areas are coincidentally the areas with minimal RORs, and the corresponding expansion ratio  $\alpha$  is least. According to their definitions, effective propagation distance  $\Xi$  increases faster, and effective transverse distance  $\varepsilon'$  is greater, which lead to faster spectral shift. When the amplitude of undulation

increases, the contrast between the expansion ratio at these areas  $\alpha = (a - b)/(a - b \cos \varphi_0)$  and in other positions is more evident, resulting in more striking difference about the speed of spectral shift at different positions. Finally, by comparing Figs. 7(a1, b1, c1) (or Figs. 7(a2, b2, c2), or Figs. 7(a3, b3, c3)), one may also observe that no-shift line and blue-shift area expand faster with the increase of initial phase, and on-axis blue shift also increases faster with greater  $\varphi_0$  (most typical in Figs. 7(a3, b3, c3)). Since the different initial phase  $\varphi_0$  essentially corresponds to different relation between  $r_0$  and  $r(t)$ , and consequently leads to different evolution of effective propagation distance  $\Xi$  and effective transverse distance  $\varepsilon'$ , it also influences distribution of spectral shift, such as blue-shift area, speed of longitudinal and transverse spectral shift, etc.

## V. CONCLUSION

We have studied Wolf effect of light on arbitrary SORs. Under the paraxial approximation, the expression of the output spectrum of polychromatic partially coherent beams is derived by applying point spread function on SORs. By defining effective propagation distance and effective transverse distance, the effect of topology of SORs on spectral shift is comprehensively analyzed, compared with that in flat space. If the effective propagation distance is larger than the real correspondence, then spectral shift will be accelerated, and vice versa. Several examples are given to verify the theoretical calculation and analyses. This work generalizes the study of Wolf effect to arbitrary SORs, and offers a general method to analyze effect of topology of surface from the perspective of comparison with that in flat space.

### Appendix: Different selection of coordinates

In all previous analyses, beam propagation starts from origin where longitudinal coordinate  $t$  is zero. However, it is not necessary. A natural question arises that, does spectral shift change if coordinate system is established in different ways?

Intuitively, physics will not change by the translation of coordinate. In the following we are going to give out detailed mathematical analysis by taking both conditions into consideration. Let us start from derivation in Section II. Ansatz  $\Phi$  mentioned in Section II

should be amended as

$$\Phi_{\pm}^g(t, \varepsilon) = A_{\pm}^g r^{-1/2}(t) u_{\pm}^g(t, \varepsilon) \exp[\pm ik(t - t'_0)], \quad (26)$$

where  $t'_0 \neq 0$  is the initial longitudinal coordinate, subscript  $\pm$  denotes the forward or backward direction of beam propagation. By repeating calculation in Section II, the revised PSF can be obtained as

$$h_{\pm}^g(\varepsilon, \varepsilon', t) = \sqrt{\frac{kr'_0}{i2\pi\Xi_{\pm}r(t)}} \exp\left[\frac{ik(\varepsilon - \varepsilon')^2}{2\Xi_{\pm}}\right] \times \exp\left[\pm ik(t - t'_0) \pm \frac{i}{2k} \int_{t'_0}^t V_{\text{eff}}(t') dt'\right], \quad (27)$$

where  $r'_0 \equiv r(t'_0)$  is ROR at incident position, and  $\Xi_{\pm} = \int_{t'_0}^t r_0^2/r^2(t') dt'$  is the revised effective propagation distance. The effective potential  $V_{\text{eff}}$ , however, is the same as previous one, indicating that it is independent of propagation direction and incident position. Attention should also be paid that initial cross spectral density should be modified as

$$W_{\text{in}}(\rho_1, \rho_2, t'_0, \omega) = S_i(\omega) \exp\left(-\frac{\rho_1^2 + \rho_2^2}{4\sigma_s^2}\right) \times \exp\left[-\frac{(\rho_1 - \rho_2)^2}{2\sigma_g^2}\right], \quad (28)$$

where  $\rho = r'_0\theta$  is the proper length at the source plane (i.e., incident position  $t = t'_0$ ), since at any plane except  $t = 0$  the coordinate  $\varepsilon = r_0\theta$  is not the transverse proper length as the ROR is no longer  $r_0$ . The corresponding output spectrum now is

$$S_{\text{out},\pm}^g(x, t, \omega) = \frac{S_i(\omega)}{\Omega_{\pm}^g(t, \omega)} \exp\left[-\frac{x^2}{2\sigma_s^2\Omega_{\pm}^g(t, \omega)^2}\right], \quad (29)$$

where

$$\Omega_{\pm}^g(t, \omega) = \alpha' \left[1 + \frac{\Xi_{\pm}^2 r_0'^4}{Z_R^2(\omega) r_0^4}\right]^{1/2}, \quad (30)$$

with new expansion ratio  $\alpha' = r(t)/r'_0$ . Here we can define  $\Xi_{\pm}^g = \Xi_{\pm} r_0'^2/r_0^2$ , i.e.,  $\Xi_{\pm}^g = \int_{t'_0}^t r_0'^2/r^2(t') dt'$  is the generalized effective propagation distance. Similarly, the generalized effective transverse distance becomes  $\varepsilon_{\pm}^g = x/\alpha'$ . Obviously these two quantities are merely relevant to ROR of incident position as well as the RORs along the propagation path, both of which are irrelevant to how coordinate is chosen. Therefore changing the way we establish coordinate system will not change the calculation results of output spectrum, beam width, spectral shift, etc. This result accords with physical intuition.

## Funding

Zhejiang Provincial Natural Science Foundation of China (No. LD18A040001); the National Key Research and Development Program of China 2017YFA0304202); the National Natural Science Foundation of China (11674284); the Fundamental Research Funds for the Center Universities (2017FZA3005).

- 
- [1] D. A. Genov, S. Zhang, and X. Zhang, *Mimicking Celestial Mechanics in Metamaterials*, Nature Phys. **5**, 687-692 (2009).
  - [2] L. J. Garay, J. R. Anglin, J. I. Cirac, and P. Zoller, *Sonic Analog of Gravitational Black Holes in Bose-Einstein Condensates*, Phys. Rev. Lett. **85**, 4643-4647 (2000).
  - [3] P. O. Fedichev and U. R. Fischer, *Gibbons-Hawking Effect in the Sonic de Sitter Space-Time of an Expanding Bose-Einstein-Condensed Gas*, Phys. Rev. Lett. **91**, 240407 (2003).
  - [4] U. Leonhardt, T. G. Philbin, C. E. Kulewicz, S. Robertson, S. Hill, F. Konig, *Fibre-Optical Analogue of the Event Horizon*, Science **319**, 1367-1370 (2008).
  - [5] U. Leonhardt and P. Piwnicki, *Optics of Nonuniformly Moving Media*, Phys. Rev. A. **60**, 4301-4312 (1999).
  - [6] U. Leonhardt and P. Piwnicki, *Relativistic effects of light in moving media with extremely low group velocity*, Phys. Rev. Lett. **84**, 822-825 (2000).
  - [7] C. Sheng, H. Liu, Y. Wang, S. N. Zhu and D. A. Genov, *Trapping light by mimicking gravitational lensing*, Nature Photon. **7**, 902-906 (2013).
  - [8] I. I. Smolyaninov, *Surface Plasmon Toy Model of a Rotating Black Hole*, New J. Phys. **5**, 147 (2003).
  - [9] E. E. Narimanov and A. V. Kildishev, *Optical black hole: Broadband omnidirectional light absorber*, Appl. Phys. Lett. **95**, 041106 (2009).
  - [10] R. Schützhold and W. G. Unruh, *Hawking Radiation in an Electromagnetic Waveguide?*, Phys. Rev. Lett. **95**, 031301 (2005).
  - [11] A. Greenleaf, Y. Kurylev, M. Lassas and G. Uhlmann, *Electromagnetic Wormholes and Virtual*

- Magnetic Monopoles from Metamaterials*, Phys. Rev. Lett. **99**, 183901 (2007).
- [12] B. S. DeWitt, *Dynamical Theory in Curved Space. I. A Review of the Classical and Quantum Action Principles*, Rev. Mod. Phys. **29**, 377-397 (1957).
- [13] R. C. T. da Costa, *Quantum Mechanics of a Constrained Particle*, Phys. Rev. A **78**, 043821 (2008).
- [14] E. O. Silva, S. C. Ulhoa, F. M. Andrade, C. Filgueiras and R. G. G. Amorim, *Quantum Motion of a Point Particle in the Presence of the Aharonov-Bohm Potential in Curved Space*, Ann. Phys **362**, 739-751 (2015).
- [15] L. C. B. da Silva, C. C. Bastos, F. G. Ribeiro, *Quantum Mechanics of a Constrained Particle and the Problem of Prescribed Geometry-Induced Potential*, Ann. Phys **379**, 13-33 (2017).
- [16] N. Fujita and O. Terasaki, *Band Structure of the P, D, and G Surfaces*, Phys. Rev. B **72**, 085459 (2005).
- [17] M. Koshino and H. Aoki, *Electronic Structure of an Electron on the Gyroid Surface: A Helical Labyrinth*, Phys. Rev. B **71**, 073405 (2005).
- [18] H. Aoki, M. Koshino, D. Takeda, H. Morise and K. Kuroki, *Electronic Structure of Periodic Curved Surfaces: Topological Band Structure*, Phys. Rev. B **65**, 035102 (2001).
- [19] J. Gravesen and M. Willatzen, *Eigenstates of Möbius Nanostructures Including Curvature Effects*, Phys. Rev. A **72**, 032108 (2005).
- [20] G. Ferrari and G. Cuoghi, *Schrödinger Equation for a Particle on a Curved Surface in an Electric and Magnetic Field*, Phys. Rev. Lett. **100**, 230403 (2008).
- [21] G. Cantele, D. Ninno and G. Iadonisi, *Topological Surface States in Deformed Quantum Wires*, Phys. Rev. B **61**, 13730-13736 (2000).
- [22] M. Encinosa and L. Mott, *Curvature-Induced Toroidal Bound States*, Phys. Rev. A **68**, 014102 (2003).
- [23] J. Onoe, T. Ito, H. Shima, H. Yoshioka and S. Kimura, *Observation of Riemannian Geometric Effects on Electric States*, EuroPhys. Lett. **98**, 27001 (2012).
- [24] M. Encinosa and B. Etemadi, *Energy Shifts Resulting from Surface Curvature of Quantum Nanostructures*, Phys. Rev. A **58**, 77-81 (1998).
- [25] H. Shima, H. Yoshioka and J. Onoe, *Geometry-Driven Shift in the Tomonaga-Luttinger Exponent of Deformed Cylinders*, Phys. Rev. B **79**, 201401(R) (2009).
- [26] A. Marchi, S. Reggiani and M. Rudan, *Coherent Electron Transport in Bent Cylindrical Sur-*

- faces*, Phys. Rev. B **72**, 035403 (2005).
- [27] G. Cuoghi, G. Ferrari and A. Bertoni, *Surface Carrier Transport in Y Nanojunctions: Signatures of the Geometric Potential*, Phys. Rev. B **79**, 073410 (2009).
- [28] J. Onoe, T. Nakayama, M. Aono and T. Hara, *Structural and Electrical Properties of an Electron-Beam-Irradiated C<sub>60</sub> Film*, Appl. Phys. Lett **82**, 595-597 (2003).
- [29] S. Batz and U. Peschel, *Linear and Nonlinear Optics in Curved Space*, Phys. Rev. A **78**, 043821 (2008).
- [30] S. Batz and U. Peschel, *Solitons in Curved Space of Constant Curvature*, Phys. Rev. A **81**, 053806 (2010).
- [31] G. D. Valle, and S. Longhi, *Geometric Potential for Plasmon Polaritons on Curved Surfaces*, J. Phys. B: At. Mol. Opt. Phys. **43**, 051002 (2010).
- [32] R. Bekenstein, J. Nemirovsky, I. Kaminer, and M. Segev, *Shape-Preserving Accelerating Electromagnetic Wave Packets in Curved Space*, Phys. Rev. X **4**, 011038 (2014).
- [33] A. Patsyk, M. A. Bandres, R. Bekenstein, and M. Segev, *Observation of Accelerating Wave Packets in Curved Space*, Phys. Rev. X **8**, 011001 (2018).
- [34] E. Lustig, M. I. Cohen, R. Bekenstein, G. Harari, M. A. Bandres, and M. Segev, *Curved-Space Topological Phases in Photonic Lattices*, Phys. Rev. A **96**, 041804(R) (2017).
- [35] R. Spittel, P. Uebel, H. Bartelt, and M. A. Schmidt, *Curvature-Induced Geometric Momenta: the Origin of Waveguide Dispersion of Surface Plasmons on Metallic Wires*, Opt. Exp. **23**, 12174-12188 (2015).
- [36] C. Conti, *Localization and Shock Waves in Curved Manifolds*, Sci. Bull. **61**, 570-575 (2016).
- [37] K. -B. Hong, C. -Y. Lin, T. -C. Chang, W. -H. Liang, Y. -Y. Lai, C. -M. Wu, Y. -L. Chuang, T. -C. Lu, C. Conti, and R. -K. Lee, *Lasing on Nonlinear Localized Waves in Curved Geometry*, Opt. Exp. **25**, 29068-29077 (2017).
- [38] V. H. Schultheiss, S. Batz, A. Szameit, F. Dreisow, S. Nolte, A. Tünnermann, S. Longhi, and U. Peschel, *Optics in Curved Space*, Phys. Rev. Lett. **105**, 143901 (2010).
- [39] V. H. Schultheiss, S. Batz, and U. Peschel, *Hanbury Brown and Twiss measurements in curved space*, Nat. Photon. **10**, 106-110 (2016).
- [40] C. Xu, A. Abbas, L. -G. Wang, S. -Y. Zhu and M. S. Zubairy, *Wolf Effect of Partially Coherent Light Fields in Two-Dimensional Curved Space*, Phys. Rev. A **97**, 063827 (2018).
- [41] E. Wolf, *Invariance of the Spectrum of Light on Propagation*, Phys. Rev. Lett. **56**, 1370-1372

- (1986).
- [42] E. Wolf, *Non-Cosmological Redshifts of Spectral Lines*, Nature **326**, 363-365 (1987).
- [43] E. Wolf and D. F. V. James, *Correlation-Induced Spectral Changes*, Reports on Progress in Physics **59**, 771-818 (1996).
- [44] T. A. Leskova, A. A. Maradudin, A. V. Shchegrov, and E. R. Méndez, *Spectral Changes of Light Scattered from a Bounded Medium with a Random Surface*, Phys. Rev. Lett. **79**, 1010-1013 (1997).
- [45] M. F. Bocko, D. H. Douglass, and R. S. Knox, *Observation of Frequency Shifts of Spectral Lines Due to Source Correlations*, Phys. Rev. Lett. **58**, 2649-2651 (1987).
- [46] R. W. Schoonover, R. Lavarello, M. L. Oelze, and P. S. Carney, *Observation of Generalized Wolf Shifts in Short Pulse Spectroscopy*, Appl. Phys. Lett. **98**, 251107 (2011).
- [47] R. Zhu, S. Sridharan, K. Tangella, A. Balla, and G. Popescu, *Correlation-Induced Spectral Changes in Tissues*, Opt. Lett. **36**, 4209-4211 (2011).
- [48] D. Zhao, O. Korotkova, and E. Wolf, *Application of Correlation-Induced Spectral Changes to Inverse Scattering*, Opt. Lett. **32**, 3483-3485 (2007).
- [49] G. M. Morris and D. Faklis, *Effects of Source Correlation on the Spectrum of Light*, Opt. Commun. **62**, 5-11 (1987).
- [50] D. Faklis and G. M. Morris, *Spectral Shifts Produced by Source Correlations*, Opt. Lett. **13**, 4-6 (1988).
- [51] J. -J. Greffet, R. Carminati, K. Joulain, J. -P. Mulet, S. Mainguy, and Y. Chen, *Coherent Emission of Light by Thermal Sources*, Nature **416**, 61-64 (2002).
- [52] H. C. Kandpal, *Experimental Observation of the Phenomenon of Spectral Switch*, J. Opt. A. **3**, 296-299 (2001).
- [53] S. Anand, B. K. Yadav, and H. C. Kandpal, *Experimental Study of the Phenomenon of  $1 \times N$  Spectral Switch Due to Diffraction of Partially Coherent Light*, J. Opt. Soc. Am. A. **19**, 2223-2228 (2002).